The Extent on the Nanoscale of Pt–Skin Effects on Oxygen Reduction and Its Influence on Fuel Cell Power

ARTICLE *in* THE JOURNAL OF PHYSICAL CHEMISTRY C · NOVEMBER 2010

Impact Factor: 4.77 · DOI: 10.1021/jp107054u

4 AUTHORS, INCLUDING:

Joelma Perez
University of São Paulo
43 PUBLICATIONS **1,001** CITATIONS
SEE PROFILE

Hebe de las Mercedes Villullas
São Paulo State University
44 PUBLICATIONS **715** CITATIONS
SEE PROFILE

The Extent on the Nanoscale of Pt-Skin Effects on Oxygen Reduction and Its Influence on Fuel Cell Power

Arthur R. Malheiro,[†,§] Joelma Perez,[†,||] Elisabete I. Santiago,[‡] and H. Mercedes Villullas*[,†]

Departamento de Físico-Química, Instituto de Química, Universidade Estadual Paulista - UNESP, Araraquara (SP) 14800-900 Brazil, and Instituto de Pesquisas Energéticas e Nucleares - IPEN/CNEN, São Paulo (SP) 05508-000, Brazil

Received: July 28, 2010; Revised Manuscript Received: October 20, 2010

Carbon-supported PtFe nanoparticles having similar overall composition (3:1), crystallinity, and average particle diameter were prepared with and without a Pt-skin layer and used to evaluate the extent, on the nanometer scale, of Pt-skin effects on the activity for oxygen reduction. In this study, we show that when most of the relevant properties of the catalysts are kept alike, there is an increase of about 2-fold in the intrinsic activity for oxygen reduction that can be ascribed to Pt-skin effects. It is also demonstrated that the activity improvement produced by the presence of a Pt-skin surface is, however, insufficient to generate significant differences on the power density of a single proton exchange membrane fuel cell.

1. Introduction

Meeting the increasing energy demand has become a central issue for sustainable growth and development, while the environmental impact of using fossil fuels is nowadays painfully clear. As result, the importance of research on different aspects of alternative and renewable energy sources has grown considerably.

Fuel cells are clean and efficient devices that allow the conversion of chemical energy into electricity from the oxidation of the fuel at the anode half-cell and the reduction of oxygen at the cathode side. Among the different fuel cell types, the proton exchange membrane fuel cell (PEMFC) has been extensively investigated over the last two decades. While PEMFCs are regarded as the most promising for vehicle and portable applications, widespread generation of electrical power using these devices is not yet feasible. The slow kinetics of the oxygen reduction reaction (ORR) has remained up until now one of the sources of severe power losses.[1]

While Pt has the highest catalytic activity for the ORR among all pure metals, more efficient electrocatalysts are still needed for PEMFC cathodes to overcome the limitations imposed by the sluggish ORR kinetics. Although other approaches have been used, the search for larger catalytic activities has involved mostly studies of bimetallic systems using Pt alloyed with first-row transition metals, which, in many cases, exhibited significantly higher catalytic activities for ORR than pure Pt. Different explanations for the enhanced activity of Pt alloys have been considered. Jalan and Taylor[2] suggested that the Pt−Pt nearest-neighbor distance was the dominant feature affecting ORR catalytic activity. Other authors proposed that OH adsorption occurring at lower potentials on the more reactive transition metal atoms would prevent adsorption of other OH groups on the surface Pt atoms, which would then remain available for the ORR.[3] A significant enhancement of catalytic activity for ORR was observed by Toda et al.[4] for sputtered films of Pt alloyed with Ni, Co, and Fe, and it was ascribed to the fact that their alloys were covered with a few Pt monolayers (that was called "Pt-skin"), in which the underlying alloy would cause an increased d-electron vacancy. Since then, other authors also have suggested that the formation of a Pt-skin layer on bimetallic surfaces would enhance the activity for ORR.[5] Pt surface layers on Pt−M (M = Fe, Ni, and Co) polycrystalline alloys were obtained by thermal treatments that promoted Pt segregation.[5−7] Studies of the ORR carried out on those extended surfaces showed that the systems with a Pt-skin were the most active.[6,7] It has also been reported that (111) Pt_3Ni single crystal surfaces covered by a Pt layer exhibit extraordinarily high ORR activities.[8] However, it is not clear if the ORR enhancement observed on Pt−M extended surfaces would occur to a similar extent on the nanometer scale, that is, on carbon-supported alloys in the fuel cell cathodes. In fact, recent studies on unsupported Pt_3Ni nanoparticles shaped as truncated-octahedrals, which had a predominant (111) surface structure, showed less than 10% of the enhancement effect observed on the extended material.[9] Other methods, such as electrochemically dealloying the transition metal[10,11] and galvanic displacement of underpotentially deposited (UPD) Cu,[12−15] were used to obtain Pt surface layers on carbon-supported nanoparticles. Nevertheless, leaching out the second metal from the surface (dealloying)[10,11] or depositing a Pt shell on particles of other metals or alloys[12−15] involve changing the overall composition of the catalyst, in some cases in an uncontrolled fashion.

In general, the catalytic enhancement of the ORR produced by the presence of a Pt-skin have been explained in terms of lattice contractions[16,17] and electronic effects.[4] However, alloying Pt with a 3d transition metal might promote similar effects, that is, changes in the Pt−Pt distance due to lattice contraction and an increase in the Pt d-band vacancy.[2,18,19] Thus, to assess the extent of Pt-skin effects on the nanometer scale, it is desirable to compare carbon-supported catalysts with and without a Pt-skin but having otherwise similar properties. To the best of our knowledge, studies of that kind have never been published.

* To whom correspondence should be addressed. Tel.: +55 16 33016653. Fax: +55 16 33016692. E-mail: mercedes@iq.unesp.br.
† Universidade Estadual Paulista.
‡ Instituto de Pesquisas Energéticas e Nucleares.
§ Present address: Rhodia Poliamida e Especialidades LTDA, Paulínia (SP), Brazil.
|| Present address: Instituto de Química de São Carlos, USP, São Carlos (SP), Brazil.

10.1021/jp107054u
Published on Web 11/04/2010

In this work, we evaluated Pt-skin effects on the ORR activity of carbon-supported PtFe nanocatalysts having similar overall composition (3:1), mean particle diameter, and crystallinity, using conventional electrochemical techniques (rotating disk electrode) and polarization curves obtained in single PEMFCs. While a nearly 2-fold increase in ORR intrinsic activity, which can be attributed to Pt-skin effects, was observed, it did not have a substantial impact on the single cell polarization response.

2. Experimental Methods

To prepare nanocatalysts with similar properties but different surface structure, that is, with and without a Pt-skin, two different synthesis procedures were adopted. In both cases, PtFe nanoparticles were obtained first in colloidal state and then supported on high surface area carbon (Vulcan XC-72, Cabot). The total metal loading (Pt + Fe) was 20 wt %.

On one hand, a reverse microemulsion method was used because it allows good control of particle size.[20] For that, *n*-heptane was used as the oil phase, and PtFe nanoparticles were synthesized using sodium bis(2-ethylhexyl)sulfosuccinate (AOT) as the surfactant and *n*-butanol as cosurfactant, as described elsewhere.[21] Briefly, an aqueous solution of H_2PtCl_6 and $FeCl_3$ (Pt:Fe 70:30 in atoms) was added to a mixture of *n*-heptane and AOT (15 wt %) under constant stirring. The water/AOT molar ratio was kept equal to 8 to obtain particles of about 3 nm. $NaBH_4$ was used as reducing agent, which was added to the microemulsion as solid. After the formation of the nanoparticles, the carbon powder was added, and the mixture was kept under constant stirring overnight. Previous studies of the electrochemical behavior as a function of composition revealed that PtFe nanocatalysts obtained in this way have both metals (Pt and Fe) on the surface.[19] This catalyst will be designated as PtFe/C.

For the preparation of the catalyst with a Pt-skin, the chosen way to promote Pt segregation to the surface was thermal treatment. Because particle growth would also take place during heating, PtFe nanoparticles of nominal composition Pt:Fe 70:30 (in atoms) were first obtained by a polyol method with an average particle diameter of about 2 nm (Figure S1 in the Supporting Information), as described elsewhere.[22,23] The synthesis was carried out by simultaneous reduction of platinum(II) acetylacetonate and iron(II) acetylacetonate (Aldrich) by 1,2-hexadecanediol in dioctyl ether, using oleic acid and oleylamine as protective agents. After separation from the reaction medium and proper washing, the nanoparticles were supported on high surface area carbon powder. The resulting catalyst was then submitted to heat treatment at 550 °C in H_2 atmosphere during 30 min. We shall designate this nanocatalyst as Pt/PtFe/C.

Catalysts were characterized by transmission electronic microscopy (TEM) using a Philips CM 200 microscope operating at 200 kV, coupled to an EDX spectrometer. The samples for the TEM analysis were prepared by ultrasonically dispersing the catalyst powders in ethanol. A drop of the suspension was applied onto a carbon-coated copper grid and dried in air.

X-ray diffraction (XRD) analysis was done using a Rigaku, model D Max 2500 PC diffractometer using Cu Kα radiation ($\lambda = 1.5406$ Å). Scans were done at 1° min^{-1} for 2θ values between 10° and 100°.

In situ dispersive X-ray absorption spectroscopy (DXAS) experiments were performed around the Pt L_3 edge (11564.25 eV). All measurements were carried out at the D06A-DXAS beamline[24] in the Brazilian Synchrotron Light Laboratory (LNLS), Brazil. The operation conditions were similar to those reported elsewhere.[25,26] The exposure time for each measured spectrum was 150 ms. A full spectrum involved 100 accumulations (frames) with 1.5 s of total acquisition time. Conversion of pixel to energy was done by comparing measurements in conventional mode with those in dispersive mode from standard foils (Pt metal). Measurements were done at constant applied potential in 0.5 mol L^{-1} H_2SO_4 solution in a spectroelectrochemical cell. The nanocatalysts were used in the form of pellets prepared by pressing a mixture of Nafion solution and the catalyst powder (Pt loading was 6 mg cm^{-2}).

The general electrochemical behavior was characterized by cyclic voltammetry in argon-saturated 0.5 mol L^{-1} H_2SO_4. The studies of catalytic activity for the ORR were done using the rotating disk electrode (RDE) technique, in O_2-saturated solution. All measurements were done in a conventional electrochemical cell, with a Pt wire counter-electrode placed in a separate compartment and a reversible hydrogen reference electrode. The catalysts were used as thin layers on a glassy carbon disk electrode (0.196 cm^2) previously polished down to 0.3 μm alumina. The total metal load (Pt + Fe) was 28 μg cm^{-2}. Solutions were prepared from analytical grade H_2SO_4 (Mallinckrodt) and ultrapure water (Milli-Q, Millipore). All experiments were done at 25 °C. A commercial Pt/C catalyst (20 wt %, E-TEK) was used as a reference sample.

Catalyst layers of gas diffusion electrodes for single PEMFC were prepared as described elsewhere.[27] Both electrodes, anode (Pt/C, 20 wt % E-TEK) and cathode (PtFe/C or Pt/PtFe/C catalysts), were prepared with a total metal loading of 0.4 mg cm^{-2}. A 35.5 wt % of Nafion (5 wt % solution in a mixture of alcohols, DuPont) was applied to the catalyst layer. The gas diffusion layer consisted of carbon powder (Vulcan XC-72R, Cabot) with 15 (w/w) polytetrafluoroethylene (PTFE, TE-306A, DuPont) deposited onto a carbon cloth (PWB-3, Stackpole). Membrane and electrode assemblies (MEA's) were prepared by hot pressing the anode and the cathode to a Nafion (H^+, N115, DuPont) membrane at 125 °C and 1000 kgf cm^{-2} during 2 min. Fuel cell polarization curves were measured galvanostatically with the single cell at 80 °C, using pure water saturated hydrogen and oxygen at 95 and 85 °C, respectively. All measurements were performed at 1 atm of overall pressure.

3. Results and Discussion

Typical TEM images taken with low magnification to give a general view of the materials are shown in Figure 1 and evidence that, for both catalysts, the nanoparticles are well distributed on the carbon support. The average particle diameters were 3.0 ± 0.4 and 3.4 ± 0.6 nm, for PtFe/C and Pt/PtFe/C, respectively. The particle diameter distribution histograms are shown in Figure S2. The actual compositions of the nanocatalysts were determined by EDX analysis and were found to be Pt:Fe 73:27 for PtFe/C and 75:25 for Pt/PtFe/C.

The structural properties were studied by X-ray diffraction. For both samples, the diffraction patterns show broad diffraction peaks associated with the face centered cubic (fcc) structure of Pt (JCPDS 4-802), as shown in Figure 2. Scherrer's equation was used to calculate the mean crystallite size. For that, the [220] peak of the Pt fcc structure was used (because the broad carbon signal does not interfere in this region). The mean crystallite diameter was found to be 2.5 nm for the PtFe/C catalyst and 2.2 nm for Pt/PtFe/C. For both catalysts, diffraction peaks are shifted toward higher 2θ values as compared to those of Pt/C. The shift in peak position provides evidence of the lattice contraction caused by the partial substitution of Pt by Fe atoms in the Pt fcc structure and demonstrates the presence

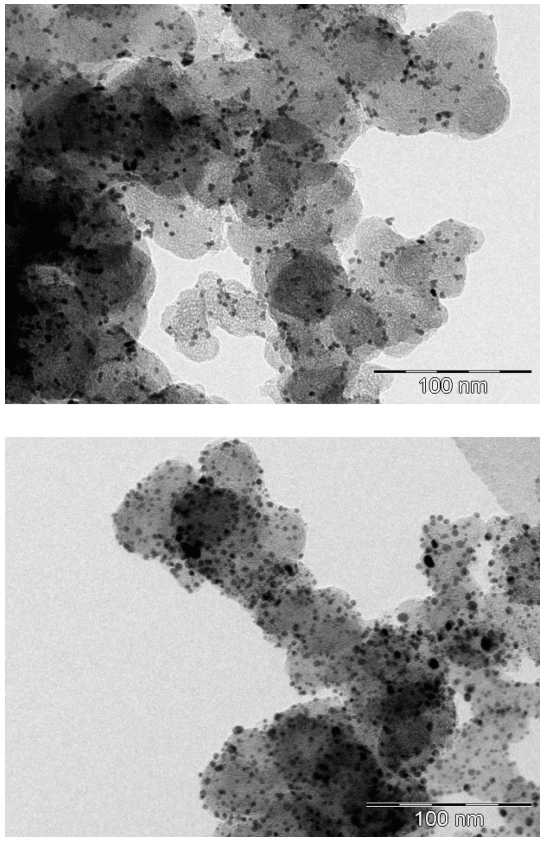

Figure 1. TEM micrographs of the carbon-supported nanonocatalysts: (a) PtFe/C; (b) Pt/PtFe/C.

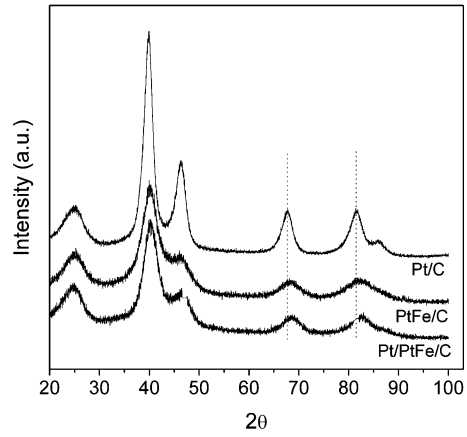

Figure 2. X-ray diffraction patterns of the carbon-supported nanonocatalysts, as indicated. The pattern for Pt/C is included for comparison.

of a PtFe alloyed phase. For the PtFe/C catalyst, the positions of the diffraction peaks and the lattice parameter (3.892 Å) are in agreement with the values expected for a PtFe solid solution with composition close to the nominal value (Pt:Fe 70:30).[4,19] For the Pt/PtFe/C sample, the diffraction signals appear at much larger 2θ values. For instance, the [220] reflection, which for a 3:1 alloy should be observed at 2θ of 67.9°, is centered at 68.5°. This 2θ value corresponds to a lattice constant (3.872 Å) smaller than that of an equimolar PtFe solid solution (3.877 Å, PDF 29-717). Thus, according to the XRD data, the alloyed phase in the Pt/PtFe/C nanocatalyst contains a much larger amount of Fe than the overall chemical composition, which indicates that more than one-half of the Pt atoms were segregated to the surface. Combining the composition of the Fe-rich alloy,

TABLE 1: Physical Properties of Nanocatalysts

catalyst	Pt:Fe (nominal)	Pt:Fe (EDX)	particle size TEM (nm)	σ	crystallite size XRD (nm)	2θ [220] peak
PtFe/C	70:30	73:27	3.0 ± 0.4	0.14	2.5	68.1
Pt/PtFe/C	70:30	75:25	3.4 ± 0.6	0.18	2.2	68.5

calculated using Vegard's law, and the average particle diameter, the estimated thickness of the Pt-skin surface layer was about 2 monolayers.

The results of the EDX, TEM, and XRD characterizations are summarized in Table 1. It is important to note that overall composition, average nanoparticle diameter, polydispersity index (σ = standard deviation/mean value), and average crystallite size are very similar for both samples.

Dispersive X-ray absorption spectroscopy (DXAS) was used to probe the electronic characteristics of electrocatalysts under in situ electrochemical conditions. Measurements were done around the Pt L_3 edge (11564.25 eV), and the analysis of white lines was done by using the method of Shukla et al.[28,29] The absorption spectra were fitted by an arc tangent function, which was subtracted from the experimental data, and the result was fitted by a Lorentzian function. As expected, both samples showed an increase of the white line intensity for increasing applied potential, resulting from the adsorption of oxygenated species on the Pt surface. Figure 3 shows the normalized Pt L_3 absorption edge for both nanocatalysts. For all applied potentials (0.4, 0.6, 0.8, and 1.0 V vs RHE), the white line intensity was larger for the Pt/PtFe/C catalyst. It is known that an increase in the Pt L_3 peak intensity reflects an increase in the Pt d-band vacancy.[30,31] In addition, systematic studies of composition effects for carbon supported PtFe nanoparticles of same size have shown that the white line intensity increases almost linearly with the amount of Fe in the alloy.[32] Thus, data of Figure 3 are consistent with a larger amount of Fe in the alloy in the Pt/PtFe/C sample and provide further evidence of the presence of Pt-skin surface layer.

The electrochemical properties of the nanocatalysts were examined by cyclic voltammetry (CV) in argon-saturated 0.5 mol L^{-1} H_2SO_4. The curves obtained at 50 mV s^{-1}, in the potential range of 0.05−0.8 V, are shown in Figure 4. The shape of the curve for the Pt/PtFe/C sample is more similar to that of Pt/C, and the charge of hydrogen adsorption/desorption is much larger than for the PtFe/C catalyst. That charge, integrated after accounting for the double layer contribution, is directly proportional to the amount of Pt on the surface because adsorption of UPD hydrogen on Fe is inhibited by the presence of oxide

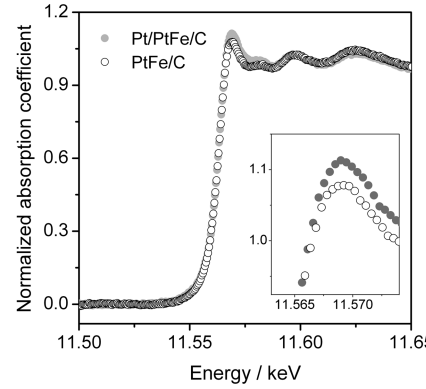

Figure 3. Normalized Pt L_3 absorption edge for PtFe/C and Pt/PtFe/C. Applied potential: 0.80 V.

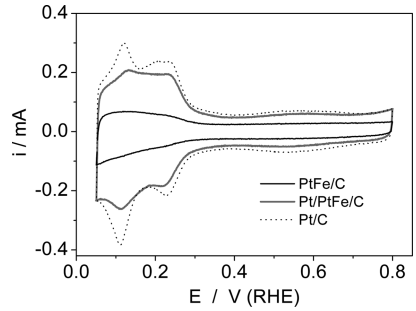

Figure 4. Cyclic voltammetry curves obtained at 50 mV s^{-1} in argon-saturated 0.5 mol L^{-1} H_2SO_4 solution. The curve for Pt/C is shown for comparison.

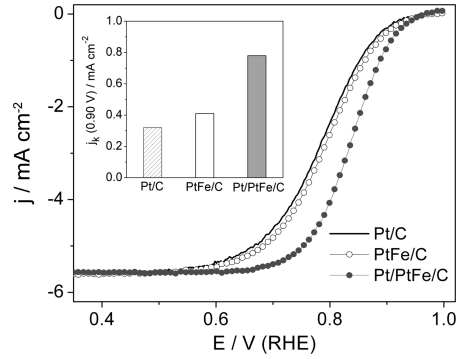

Figure 5. Polarization curves for the ORR on PtFe/C and Pt/PtFe/C nanocatalysts. Rotation rate: 2500 rpm. Sweep rate: 5 mV s^{-1}. Electrolyte: O_2-saturated 0.5 mol L^{-1} H_2SO_4 solution. The curve for Pt/C is shown for comparison. Inset: Kinetic current densities at 0.90 V.

species.[33] Because both catalysts have similar average nanoparticle diameter and polydispersity index, the larger hydrogen adsorption/desorption charges provide additional proof of the presence of a Pt-skin on the Pt/PtFe/C catalyst.

A typical set of oxygen reduction polarization curves is shown in Figure 5, where current densities are normalized to the geometric area of the glassy carbon substrate. The polarization curve for a commercial Pt/C catalyst (3.4 ± 1.2 nm)[34] is included for comparison. At any given potential, the rate of an electrochemical reaction will be determined by the exchange current density and the Tafel slope. Because of the uncertainties in the evaluation of the exchange current density that result from the large overpotential of the ORR, comparisons of activity are often made in terms of kinetic current densities measured at 0.9 V, which can be calculated by using the equation:[35]

$$\frac{1}{j} = \frac{1}{j_k} + \frac{1}{j_L}$$

where j_k and j_L are, respectively, the kinetic and diffusion controlled current densities. It is evident that while both Fe containing catalysts are more active than Pt/C, the one with Pt-skin surface shows the larger ORR activity enhancement. The kinetic current density at 0.90 V for the Pt/PtFe/C nanocatalyst was found to be larger than for PtFe/C by a factor of nearly 2 (inset of Figure 5), in agreement with data for Pt_3Fe extended surfaces.[7] The mass-transport corrected Tafel plots showed slopes close to -0.06 V dec^{-1} in the low current densities region (Figure S3) and -0.12 V dec^{-1} at high current densities, indicating that the reaction mechanism is likely to be the same as on pure Pt electrodes.[36,37]

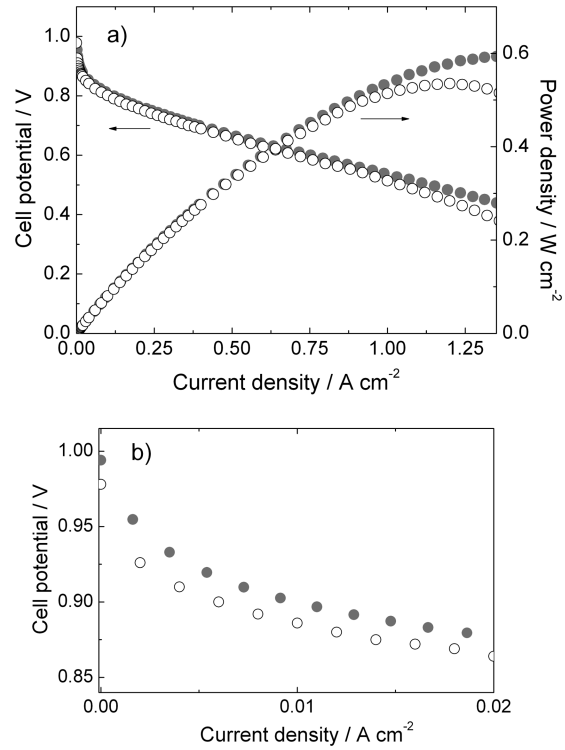

Figure 6. (a) PEMFC polarization data obtained at 80 °C with Pt/C as anode catalyst and PtFe/C (open symbols) or Pt/PtFe/C as cathode catalyst. (b) Polarization data in the activation-controlled potential region.

The polarization curves for single cells using the PtFe/C or Pt/PtFe/C as cathode catalyst are depicted in Figure 6a. The differences in ORR activity are apparent in the fuel cell polarization curves in the region of activation control (Figure 6b). Comparisons of activity are, in this case, usually made in terms of current densities measured at 0.9 V. At that potential, the measured current densities were 6 mA cm^{-2} for the cell with PtFe/C as cathode material and 9 mA cm^{-2} for Pt/PtFe/C. As expected, the Pt-skin effect produced an enhancement in the current density measured in the fuel cell polarization curve that is similar to that observed in the RDE experiments. Also, the open circuit potential is ca. 20 mV higher for the cell with Pt/PtFe/C in the cathode. Another important parameter, because of its practical implications, is the so-called mass activity, which is the current density per mg of Pt. It must be noted, however, that in the present case both cathodes have the same amount of Pt because they were prepared with identical load (0.4 mg cm^{-2}) of catalysts having the same overall composition. The Tafel slopes in the region of activation control were 0.065 and 0.073 V dec^{-1} for PtFe/C and Pt/PtFe/C, respectively (Figure S4).

An additional aspect of the results presented in Figure 6a is that the enhancement of ORR catalytic activity, which can be attributed to the presence of the Pt-skin surface, is not reflected in the single cell power response. For instance, the power density of the single cell is nearly the same for both cathode materials, with a difference of less than 5% for current densities of 1 A/cm^2.

Although Pt layers deposited on particles of other metals or alloys[12−15] might allow lowering the Pt content in ORR catalysts, which is obviously important and highly desirable, the 2- or 3-fold increase in catalytic activity usually observed for that kind of materials[38] is unlikely to improve PEMFCs performance in the potential region of practical interest. The rather insignificant impact of an almost 2-fold increase in ORR intrinsic

activity on power density shown in Figure 6a is, in fact, in excellent agreement with theoretical simulations on the influence of the ORR exchange current density on fuel cell power.[39]

4. Conclusions

Carbon-supported PtFe nanocatalysts were prepared with and without a Pt-skin while keeping other relevant properties alike. Thus, the extent of the enhancement of the activity for oxygen reduction due to the presence of a Pt-skin was evaluated in the nanometer scale in the absence of overall composition changes and particle size effects. The presence of a Pt-skin layer was evidenced by X-ray diffraction, dispersive X-ray absorption spectroscopy, and cyclic voltammetry data. It was found that a nearly 2-fold enhancement of intrinsic activity for oxygen reduction was promoted by Pt-skin effects. Nevertheless, while nanocatalysts with a Pt-skin layer might allow reducing the Pt content, the results obtained in single PEMFCs using PtFe/C and Pt/PtFe/C as cathode catalysts indicate that a nearly 2-fold increase in ORR catalytic activity rendered by Pt-skin effects is not yet sufficient to produce noticeable increases in fuel cell power density in the potential region of practical interest.

Acknowledgment. Thanks are due to Brazilian Agencies FAPESP (07/54434-0), CNPq (480662/2007-0; 305106/2007-4), and FINEP (01.06.0939.00) for financial support, and to the Brazilian Synchrotron Light National Laboratory (LNLS) for assisting the DXAS measurements.

Supporting Information Available: TEM image of catalyst used for heat treatment, particle diameter distribution histograms, Tafel plots from RDE experiments, and Tafel plots from PEMFCs polarization data. This material is available free of charge via the Internet at http://pubs.acs.org.

References and Notes

(1) Costamagna, P.; Srinivasan, S. *J. Power Sources* **2001**, *102*, 242–252.
(2) Jalan, V.; Taylor, E. J. *J. Electrochem. Soc.* **1983**, *130*, 2299–2301.
(3) Paulus, U. A.; Wokaun, A.; Scherer, G. G.; Schmidt, T. J.; Stamenkovic, V.; Radmilovic, V.; Markovic, N. M.; Ross, P. N. *J. Phys. Chem. B* **2002**, *106*, 4181–4191.
(4) Toda, T.; Igarashi, H.; Watanabe, M. *J. Electroanal. Chem.* **1999**, *460*, 258–262.
(5) Stamenkovic, V.; Schmidt, T. J.; Ross, P. N.; Markovic, N. M. *J. Electroanal. Chem.* **2003**, *554*, 191–199.
(6) Stamenkovic, V. R.; Mun, B. S.; Mayrhofer, K. J. J.; Ross, P. N.; Markovic, N. M. *J. Am. Chem. Soc.* **2006**, *128*, 8813–8819.
(7) Stamenkovic, V. R.; Mun, B. S.; Arenz, M.; Mayrhofer, K. J. J.; Lucas, C. A.; Wang, G.; Ross, P. N.; Markovic, N. M. *Nat. Mater.* **2007**, *6*, 241–247.
(8) Stamenkovic, V. R.; Fowler, B.; Mun, B. S.; Wang, G.; Ross, P. N.; Lucas, C. A.; Markovic, N. M. *Science* **2007**, *315*, 493–497.
(9) Wu, J.; Zhang, J.; Peng, Z.; Yang, S.; Wagner, F. T.; Yang, H. *J. Am. Chem. Soc.* **2010**, *132*, 4984–4985.
(10) Koh, S.; Strasser, P. *J. Am. Chem. Soc.* **2007**, *129*, 12624–12625.
(11) Mani, P.; Srivastava, R.; Strasser, P. *J. Phys. Chem. C* **2008**, *112*, 2770–2778.
(12) Zhang, J.; Mo, Y.; Vukmirovic, M. B.; Klie, R.; Sasaki, K.; Adzic, R. R. *J. Phys. Chem. B* **2004**, *108*, 10955–10964.
(13) Adzic, R. R.; Zhang, J.; Sasaki, K.; Vukmirovic, M. B.; Shao, M.; Wang, J. X.; Nilekar, A. U.; Mavrikakis, M.; Uribe, F. *Top. Catal.* **2007**, *46*, 249–262.
(14) Shao, M. H.; Sasaki, K.; Marinkovic, N. S.; Zhang, L.; Adzic, R. R. *Electrochem. Commun.* **2007**, *9*, 2848–2853.
(15) Ghosh, T.; Vukmirovic, M. B.; DiSalvo, F. J.; Adzic, R. R. *J. Am. Chem. Soc.* **2010**, *132*, 906.
(16) Xu, Y.; Ruban, A. V.; Mavrikakis, M. *J. Am. Chem. Soc.* **2004**, *126*, 4717–4725.
(17) Nilekar, A. U.; Mavrikakis, M. *Surf. Sci.* **2008**, *602*, L89–L94.
(18) Mukerjee, S.; Srinivasan, S.; Soriaga, M. P.; McBreen, J. *J. Electrochem. Soc.* **1995**, *142*, 1409–1422.
(19) Malheiro, A. R.; Perez, J.; Villullas, H. M. *J. Electrochem. Soc.* **2009**, *156*, B51–B58.
(20) Godoi, D. R. M.; Perez, J.; Villullas, H. M. *J. Electrochem. Soc.* **2007**, *154*, B474–B479.
(21) Malheiro, A. R.; Varanda, L. C.; Perez, J.; Villullas, H. M. *Langmuir* **2007**, *23*, 11015–11020.
(22) Santiago, E. I.; Varanda, L. C.; Villullas, H. M. *J. Phys. Chem. C* **2007**, *111*, 3146–3151.
(23) Malheiro, A. R.; Perez, J.; Villullas, H. M. *J. Power Sources* **2010**, *195*, 3111–3118.
(24) Tolentino, H. C. N.; Cezar, J. C.; Watanabe, N.; Piamonteze, C.; Souza-Neto, N. M.; Tamura, E.; Ramos, A. Y.; Neueschwander, R. *Phys. Scr.* **2005**, *T115*, 977–979.
(25) Godoi, D. R. M.; Perez, J.; Villullas, H. M. *J. Phys. Chem. C* **2009**, *113*, 8518–8525.
(26) Godoi, D. R. M.; Perez, J.; Villullas, H. M. *J. Power Sources* **2010**, *195*, 3394–3401.
(27) Paganin, V. A.; Ticianelli, E. A.; Gonzalez, E. R. *J. Appl. Electrochem.* **1996**, *26*, 297–304.
(28) Shukla, A. K.; Raman, R. K.; Choudhury, N. A.; Priolkar, K. R.; Sarode, P. R.; Emura, S.; Kumashiro, R. *J. Electroanal. Chem.* **2004**, *563*, 181–190.
(29) Sousa, R.; Colmati, F.; Ciapina, E. G.; Gonzalez, E. R. *J. Solid State Electrochem.* **2007**, *11*, 1549–1557.
(30) Mukerjee, S.; Srinivasan, S.; Soriaga, M. P.; McBreen, J. *J. Phys. Chem.* **1995**, *99*, 4577–4589.
(31) Mukerjee, S.; Srinivasan, S.; Soriaga, M. P.; McBreen, J. *J. Electrochem. Soc.* **1995**, *142*, 1409–1422.
(32) Malheiro, A. R.; Perez, J.; Villullas, H. M. *J. Power Sources* **2010**, *195*, 7255–7258.
(33) Conway, B. E.; Jerkiewicz, G. *Electrochim. Acta* **2000**, *45*, 4075–4083.
(34) Paulus, U. A.; Wokaun, A.; Scherer, G. G.; Schmidt, T. J.; Stamenkovic, V.; Markovic, N. M.; Ross, P. N. *Electrochim. Acta* **2002**, *47*, 3787.
(35) Gileadi, E. *Electrode Kinetics. For Chemists, Chemical Engineers, and Materials Scientists*; VCH: New York, 1993; p 5.
(36) Tarasevich, M. R.; Sadkowski, A.; Yeager, E. In *Comprehensive Treatise in Electrochemistry*; Bockris, J. O. M., Conway, B. E., Yeager, E., Khan, S. U. M., White, R. E., Eds.; Plenum: New York, 1983; p 301.
(37) Perez, J.; Villullas, H. M.; Gonzalez, E. R. *J. Electroanal. Chem.* **1997**, *435*, 179–187.
(38) Wang, J. X.; Inada, H.; Wu, L.; Zhu, Y.; Choi, Y. M.; Liu, P.; Zhou, W. P.; Adzic, R. R. *J. Am. Chem. Soc.* **2009**, *131*, 17298–17302.
(39) Srinivasan, S. *Fuel Cells. From Fundamentals to Applications*; Springer: New York, 2006; pp 215−220.

JP107054U